Monte Carlo modeling on primary damage generation induced by ions in solid materials

YAN Qiang[1], WU Chenbin[1], and LI Wei[1]

1. College of Nuclear Science and Technology, Harbin Engineering University, Harbin 150001, PR China（yankang84@126.com）

Abstract: Monte Carlo modeling on the interaction between ions and amorphous solid materials and the primary damage generation is presented in this paper. Based on BCA (Binary Collision Assumption), the movement of ions in materials is divided into straight segments and modeled by single elastic scattering event and continuum electronic energy loss. To deal with the elastic scattering under screened Coulomb potential, geometrical treatment in Center of Mass System is used to get scattering angle and energy transfer. The energy lost by excitation and ionization of target atoms is approximated by continuum electronic stopping power, estimated by two kinds of models based on fitting expression of experimental data. Using the implementation of collision treatment and electronic stopping power, Mersenne-Twister-algorithm-based random number generator and simple OpenGL-based visualization tool, a whole set of simulation code is established. By applying this code, trajectories and primary displacement damage were simulated and analyzed. Results showed good agreement compared with SRIM (Stopping and Range of Ions in Mater) code. Due to much better flexibility of the code presented here, the PKA spectrum, the 3-D distribution of defects and time information of PKA (Primary Knock-on Atoms) are investigated, which are not accessible using SRIM code. The code was integrated to Deeper (Damage creation and particle transport in matter) code and can serve as the primary damage generator of Multi-Scale modeling of radiation damage.

Keyword: Monte Carlo modeling; ion radiation; radiation damage; multi-scale modeling

1 Introduction

The interaction between ions and solid and damage induced by ions are essential for ion beam applications[1-3]and radiation damage research[4]. Energized ions, usually coming from accelerators, play the most important role in experimental radiation damage research, overcoming the main drawbacks of reactor neutron source radiation including the very long radiation time to get enough damage level, very high cost, activation of sample which may cause radioactive contamination (or radioactive waste) and injury to the participants and the very limited accessible research reactors. Ion radiation, especially heavy ions radiation will generate similar damage cascades as neutrons do, so it is believed that neutron induced damage can be simulated by ion radiation to investigate the mechanism of radiation damage, estimate performance of materials under the radiation circumstance and develop new radiation-resistant materials. Non-ion particles, such as neutrons and electrons, induced damage in solid begins with the generation of recoil atoms kicked out by ions (called as Primary Knock-on Atoms, PKA), the following cascade generation is caused by secondary ions in target materials and can be treated in the same way as ions radiation. So the modeling of ion induced damage is not only crucial for accelerator-based radiation damage experiment, but also fundamental for the whole research field of radiation damage[5].

Many tools based on Monte Carlo method with the function of simulating behavior of ions in solids can be found, such as some general-purpose tools like Fluka[6] and Geant4[7], specific tools like Marlowe[8], SRIM[9,10], Simnra[11], and Tridyn_Hzdr[12]. Fluka and Geant4 are two kind of widely used tools developed by CERN, aiming at the application of high energy experiments. Poor performance was found when they were used in the energy range of MeV to simulate the damage cascade in solid. The specific tools mentioned above are all based on Binary Collision Assumption(BCA) and wildly used in the field of modeling the interaction of ions in materials and applied in ion implanting, dose evaluation, detector simulation and optimization, radiation damage and ion analyzing. In radiation damage research, Marlowe and SRIM are the two most important tools. Marlowe can model the interaction between ions and all kind of

Received date: May 10, 2016
(Revised date: July 7, 2016)

solid materials (amorphous, poly-crystal and crystal) and output very detailed description of cascade. The electronic stopping power model used in Marlowe is only valid for energy lower than 25 kev/nucleon[13], which is not high enough to simulation MeV ions. SRIM can simulate ions in very wide energy range(up to GeV) and output many kinds of parameters, such as ion profile and range, damage profile, sputtering and back-scattering yield and energy deposit profile, serving as a basic tool in calibrating damage level of ion radiation experiments[10]. SRIM is not open-sourced and the limited flexibility makes users difficult to get detailed information of cascade beyond the statistic results provided by SRIM. These limitations make Marlowe and SRIM not suitable for muli-scale modeling.

For multi-scale modeling, the position of every defect (interstitial atoms, I, or vacancy,V) and the time of PKA generating are two kinds primary information will be used by other tools, like kinetic Monte Carlo(KMC)[14]. But unfortunately, the existing BCA tools cannot provide those kinds of information efficiently. In this paper, based on well estimated models and data, a C++ coded tool, which well meets the demand of multi-scale modeling, is reported. The code was integrated to Deeper (Damage creation and particle transport in matter) software package, a simulation tool designed to model the transportation and damage generation of ions, electrons and neutrons.

2 Theory models

The modeling is based on BCA, which is wildly used in the simulation work of ion bombarding and relevant phenomenons, such as sputtering, back scattering and radiation damage. The basic approximation in BCA is shown in Figure 1. Ion track is divided into a series of strait segments with a length of free fight distance and independent collision points. At the collision points, the interaction between ions and crystal lattice atoms occurs and is simplified as binary collision, ignoring the influence of lattice and neighbor atoms. Ions lost energy by electronic interaction with the electrons by excitation and ionization along the free fight distance and then suffer a collision event. By collision, the direction of ions is changed and part of kinetic energy is transferred to the target atom. If the energy transferred to atom exceeds a threshold, called as the displacement energy of this kind of atom, the atom will be displaced from the lattice and become a recoil atom. After the recoil atom gets enough energy, it may cause other atoms displaced and a cascade occurs. Key information used to describe the status of ions at every collision points includes the position of ions, the momentum direction and the energy. In BCA, it's essential to process the binary collision to get the angular relationship and energy transfer before and after a collision happens, and electronic energy loss between collisions due to ionization and exciting of target atoms. If a high energy recoil atom is produced, the process of cascade generating can be simulated by treating the recoil atom as self-ion and using the same approach as injecting ions.

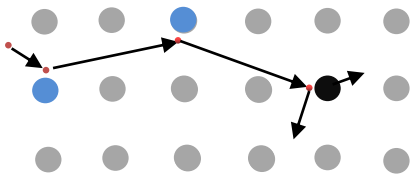

Fig.1 the demonstration of BCA.

In Fig.1, the demonstration of BCA is presented. The big gray circles are the lattice atoms (the blue ones are target atoms which can interact with ion) and the small circles are is the ion at different collision points. The arrays stand for the free flight distance, which means the distance where the ion will not encounter an effective collision. The recoil atom, marked by black color, only occurs when enough energy transferred to target atoms. To deal with the ion transportation in mater, theoretical models to process the binary collision and electronic stopping power is needed, which are presented as following. Due to the dominating importance of random number used in Monte Carlo simulation, the random number generator, together with the visualization tools, is also presented in this chapter.

2.1 The procession of binary collision

In our code, the method of processing elastic collision presented by Biersack and Haggmark in 1980 was used[15]. Basically speaking, a geometry relationship, called "scattering triangle", of trajectories of ion and recoil atom in Center of Mass (CM) System was obtained to get the term of $\cos(\theta/2)$(θ is the scattering angle in CM system) by using a very successful fitting

expression (the so-called "magic formula"), in which the impact parameter, screening effect of electrons and the energy of ions are taken into account. This expression is very convenient and efficient for numerical computation compared with other analytic results and has been used very wildly in simulation research of ions. The scattering angle θ in CM system is the key parameter in simulation, from which the energy transfer to atom can be expressed by

$$E_T = \frac{4M_1M_2}{(M_1+M_2)^2} E_k \sin^2(\frac{\theta}{2}) \quad (1)$$

where E_k is the kinetic energy of ion, M_1 is the mass of ion and M_2 is the mass of atom. The direction of ions and recoil atoms are obtained from the scattering angle in laboratory system, which can be worked out from θ by using the following expression:

$$\tan(\theta_L) = \frac{\sin(\theta)}{\cos(\theta)+\frac{M_1}{M_2}} \quad (2)$$

In our code, we used a cartesian coordinate system shown in Fig.2. The directional vector , defined as as the project in X,Y and Z direction(expressed by angles of α and φ), after collision can be expressed with the original directional vector, the scattering angle in laboratory system and the azimuth angle α_0, which is uniformly distributed from 0 to 2π.

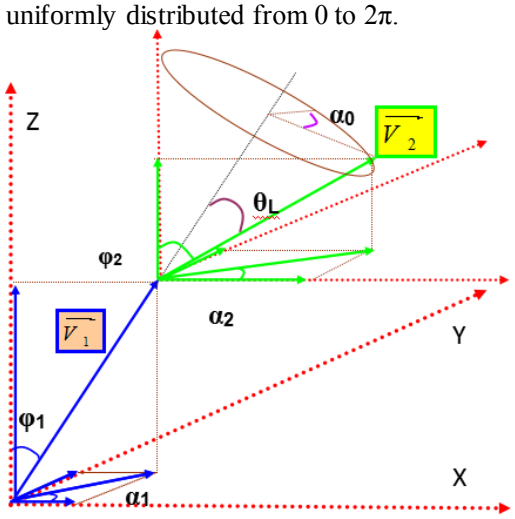

Fig.2 the directional vector of ions after an elastic collision.

The original vector of ion before collision($\vec{V}_1$) is:

$$\begin{cases} V_{1x} = \sin\varphi_1 \cos\alpha_1 \\ V_{1y} = \sin\varphi_1 \sin\alpha_1 \\ V_{1z} = \cos\varphi_1 \end{cases} \quad (3)$$

And the vector after collision ($\vec{V}_2$) can be worked out and expressed as:

$$\begin{cases} V_{2x} = \cos\theta_L \sin\varphi_1 \cos\alpha_1 - \sin\theta_L \cos\theta_L \cos\alpha_0 \cos\alpha_1 \\ \qquad -\sin\theta_L \sin\alpha_0 \sin\alpha_1 \\ V_{2y} = \cos\theta_L \sin\varphi_1 \sin\alpha_1 - \sin\theta_L \cos\theta_L \cos\alpha_0 \sin\alpha_1 \\ \qquad -\sin\theta_L \sin\alpha_0 \cos\alpha_1 \\ V_{2z} = \cos\theta_L \cos\varphi_1 + \sin\theta_L \cos\alpha_0 \sin\varphi_1 \end{cases} \quad (4)$$

where θ_L is the scattering angle in laboratory system. Same approach is used to get directional vectors of recoil atoms.

2.2 electronic stopping power

Energy lost by electronic interactions is much bigger than that by collisions with atom nuclei, especially for high energy case, where ions loss their energy mainly by electronic interactions. We calculated the energy change along the free fight distance L by expression:

$$\Delta E = -\frac{dE}{ds} L \quad (5)$$

Where dE/ds means the rate of energy loss at energy E, and it was called as electronic stopping power. Although many theoretical results exist, such as Lindhard model[16] for low energy ions and Beth-Bloch[17] formula for high energy ions, we choose fitting formula based on the experimental data for the simpleness in programming and better speed. In this work, two kinds electronic stopping power were presented. The Zeiger-Anderson model has simpler expression and better calculation efficiency and the Zeiger-Bersack can be used for higher energy case(up to 2GeV) .

2.2.1 Zeiger-Anderson stopping power

In this model, a series of fitting formula for proton (presented by H.H. Andersen and J.F. Ziegler) and Alpha particles (presented by J.F. Ziegler)are used. For protons, the fitting formula used in this work can be summarize as[18]:

$$S_p = \begin{cases} \alpha_1\sqrt{E} & (0 \le E \le 10keV) \\ \dfrac{S_L S_H}{S_L + S_H} & (10keV \le E \le 999keV) \\ \dfrac{\alpha_6}{\beta^2}\left[\ln\left(\dfrac{\alpha_7\beta^2}{1-\beta^2}\right) - \beta^2 - C - \dfrac{\delta}{2}\right] & \\ \qquad (1000keV \le E) & \end{cases} \quad (6)$$

Where E means the kinetic energy of ions, with a unit of ***kev/nucleon***, β is the velocity of ions in unit of c(velocity of light in vacuum), δ is the density effect obtained from the Sternheimer asymptotic form. The

other parameters are defined as:

$$S_L=\alpha_2 E^{0.45}$$
$$S_H=\frac{\alpha_3}{E}\ln\left(1+\frac{\alpha_4}{E}+\alpha_5 E\right) \quad (7)$$
$$C=\sum_{i=1}^{5}\alpha_{7+i}[\ln(E)]^{i-1}\left\{1-\exp\left[-2\left(\frac{10^5}{E}\right)^2\right]\right\}$$

Where a_1 to a_{12} are fitting parameters, which vary from every kinds of target elements. These parameters can be found in the book edited by H.H. Andersen and J.F. Ziegler in 1977[19].

For alpha particles, another set of fitting formula is used[18]:

$$S_\alpha=\begin{cases}\alpha_1 E^{\alpha_2} & E\le 1keV\\ \dfrac{S_L S_H}{S_L+S_H} & 1keV\le E\le 10^4 keV\\ S_1 & 10^4 keV\le E\le 2\times10^4 keV\\ \left[1-\dfrac{E-2\times10^4}{2\times10^4}\right]S_1+\left[\dfrac{E-2\times10^4}{2\times10^4}\right]4S_p & \\ \qquad 2\times10^4 keV\le E\le 4\times10^4 keV & \\ S_p & E\ge 4\times10^4 keV\end{cases} \quad (8)$$

Where E has the same meaning as above. Other parameters are defined as:

$$S_L=\alpha_1 E^{\alpha_2}$$
$$S_H=\frac{10^3\alpha_3}{E}\ln\left(1+\frac{10^3\alpha_4}{E}+\alpha_5\frac{E}{10^3}\right)$$
$$S_1=\left\{\alpha_6+\alpha_7\ln\left(\frac{1000}{E}\right)+\alpha_8\left[\ln\left(\frac{1000}{E}\right)\right]^2+\alpha_9\left[\ln\left(\frac{1000}{E}\right)\right]\right\}^3 \quad (9)$$

Where a_1 to a_9 are fitting parameters, and can be found in the book edited by Zeigler in 1977[20].

For heavy ions(Z>2), electronic stopping power are calculated from that for alpha particles using a scaling rule:

$$S_{Heavy}=\frac{(Z^*_{Heavy})^2}{(Z^*_\alpha)^2}S_\alpha \qquad Z^*=(1-\exp(-1.25x))Z$$
$$x=100\beta/Z^{2/3} \quad (10)$$

Where β is the ratio between the velocity of ion and velocity of light in vacuum.

2.2.1 Zeiger-Bersack stopping power

The main advantage of this model is that stopping power expressions for all ions except protons (including alpha particles) are based on the data of protons. So in this model, only one set of fitting parameters is needed while two sets of fitting parameters should be provided in Zeigler-Anderson model (one for proton, the other for alpha particles and heavy ions). The fitting formula [21] for protons has quite different form compared with Eq.(6) and (7)

$$S_p=\begin{cases}S_p(25)*\left(\dfrac{E}{25}\right)^{\alpha_0} & \alpha_0=\begin{cases}0.25 & Z_2\le 6\\ 0.45 & Z_2>6\end{cases}\\ \qquad E\le 25keV & \\ \dfrac{S_L S_H}{S_L+S_H} & 25keV\le E\le 10^4 keV\\ \alpha_9+\alpha_{10}\dfrac{\ln E}{E}+\alpha_{11}\left[\dfrac{\ln E}{E}\right]^2+\alpha_{12}\left[\dfrac{E}{\ln E}\right] & \\ \qquad 10^4 keV\le E\le 2\times10^6 keV & \end{cases} \quad (11)$$

With parameters defined by:

$$S_L=\alpha_1 E^{\alpha_2}+\alpha_3 E^{\alpha_4}$$
$$S_H=\frac{\alpha_5\ln\left(\dfrac{\alpha_6}{E}+\alpha_7 E\right)}{E^{\alpha_8}} \quad (12)$$

In this model, E has the same meaning as above and a_1～a_{12} are fitting parameters presented by Zeigler and Bersack in 1985[22].

The stopping power for ions heaver than proton can be calculated using scaling rule:

$$S_{ion}=\frac{S_p(\gamma Z_1)^2}{Z_p}=S_p(\gamma Z_1)^2 \quad (13)$$

γZ_1 means the effective charge of ions, which has different forms for alpha particles and heavy ions. For alpha particles, an expression presented by Zeigler *etc.* is[22]:

$$\gamma^2=1-\exp\left(-0.2865-0.1266B+0.001429B^2-0.02402B^3+0.01135B^4-0.001475B^5\right)c^2$$
$$c=1+(0.007+0.00005Z_2)\exp\left[-(7.6-\ln(E/M_1))^2\right] \quad (14)$$
$$B=\ln\frac{E}{M_1}$$

Where Z_2 is the atomic number of target and M_1 is the mass number of alpha particles. It was suggested that using Eqs.(13) and (14) to calculate the stopping

power for alpha particle with energy higher than 4***keV***, and the stopping power is proportional to the ion velocity.

For heavy ions, a much more complicated expression of γ will be used:

$$q = 1 - \exp\left(0.803 y_r^{0.3} - 1.3167 y_r^{0.6} - 0.38157 y_r - 0.008983 y_r^2\right)$$

$$y_r = \begin{cases} \dfrac{\upsilon_1}{\upsilon_0 Z^{2/3}}\left(1 + \dfrac{\upsilon_F^2}{5\upsilon_1^2}\right) & \upsilon_1 \geq \upsilon_F \\ \dfrac{0.75\upsilon_F}{\upsilon_0 Z^{2/3}}\left[1 + \left(\dfrac{2\upsilon_1^2}{3\upsilon_F^2}\right) - \dfrac{1}{15}\left(\dfrac{\upsilon_1}{\upsilon_F}\right)^4\right] & \upsilon_1 > \upsilon_F \end{cases} \quad (15)$$

Where v_F is the Fermi velocity for the target material, v_0 is the Bohr velocity, a_0 is the Bohr radius (0.529Å), and q is the degree of ionization of the ion, which is given by:

$$\gamma = q + 0.5(1-q)\frac{\upsilon_0}{\upsilon_F}\ln\left[1 + \left(\frac{2\Lambda\upsilon_F}{\alpha_0\upsilon_0}\right)^2\right]C \quad (16)$$

Where yr is effective ion velocity, Λ is the ion screening radius, which can be defined as:

$$\Lambda = \frac{2\alpha_0(1-q)^{2/3}}{Z_1^{1/3}\left(1 - \dfrac{1-q}{7}\right)} \quad (17)$$

And C is a correction factor for polarization of target atoms, expressed by:

$$C = 1 + \frac{1}{Z_1^2}(0.18 + 0.0015 Z_2)\exp\left[-\left(7.6 - \ln\frac{E}{M_1}\right)^2\right] \quad (18)$$

2.3 random number generator and visualization

Huge amount of random numbers will be used in the simulation, the quality of random number is critical for Monte Carlo simulation. Because it not easy to produce real random numbers mathematically, pseudo-random number sequence with a repeating period, which is generated by specific algorithm, is used in actual simulation. Although there are many kinds of algorithm and implementation can be found, we chose the reliable C++ implementation of Mersenne-Twister algorithm presented by Makoto Matsumoto *etc.*.[23] It was designed with consideration of the flaws in various other generators. The only parameter needed to generate random number sequence is a "random seed", which is usually set with the current time of computer to make sure different random sequences are used for different simulation. In our code, a 53-bit random number was used, with a period of 2^{53}-1 (about 10^{15}), which is long enough for our code. In the repeating period of the sequence, random numbers with very good randomness distributed uniformly in the range of (0, 1].

To visualize the trajectories of ions and secondary ions, we developed a simple 3D visualization tool based on OpenGL library[24]. Due to the powerful function of OpenGl, developers can produce graphic tool with high performance with few work of coding. In our code, the trajectories of a fixed number (specified by users, for example, 50) of incident ions were displayed in a 3D form. The displaying of trajectories can be modified by moving, rotating and magnifying. Too many trajectories to be visualized are not recommended because of very large memory cost. Users can also choose only recoil atoms to be visualized to observe only the damage.

3 Results and discussion

3.1 The validation of electronic stopping power models

To evaluate the electronic stopping power models, the stopping power (in unit of eV/Angstrom) of Fe ions in pure iron were calculated using the two kind of stopping power models presented above. The comparison of results is shown in Fig. 3. Although slight difference does exist, the electronic stopping power from two models match quite well in a very wide energy range (From a few keV to 10MeV). For Zeigler-Biersack stopping power, the electronic stopping power is assumed to be proportional to $E^{0.45}$ for low energy ion. This approximation may cause problem for the simulation of low energy ions. In the simulation, we used the Lindhard stopping power for low energy ions[25]. This stopping power model can be expressed as:

$$S_L = kE^p \quad k = \frac{1.212 Z_1^{7/6} Z_2}{\left(Z_1^{2/3} + Z_2^{2/3}\right)^{2/3} M^{1/2}} \quad (20)$$

$$p = \frac{1}{2}$$

Where Z_1 and Z_2 are the atomic number of ions and target atoms, M is the mass number of ions.

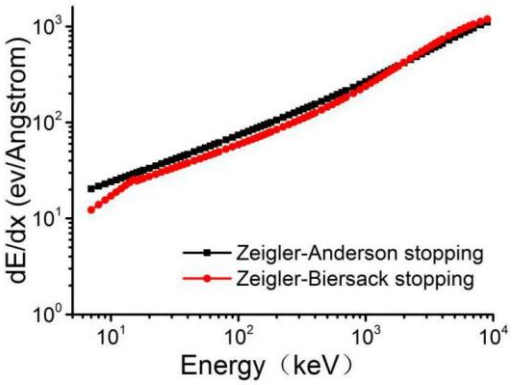

Fig.3 electronic stopping power of Fe ions in pure iron as a function of ion energy.

3.2 trajectory simulation using Deeper code

The trajectory simulation is the most important basic function of Deeper code. Many applications are based on ion trajectory simulation, such as the modeling of back-scattering Rutherford analyzing, ion therapy and channeling effect. For mutl-scale modeling, the defect generation is meaningful only when the transportation of ions is correct. We used trajectory simulation to check the validation of our code by comparison with the SRIM code.

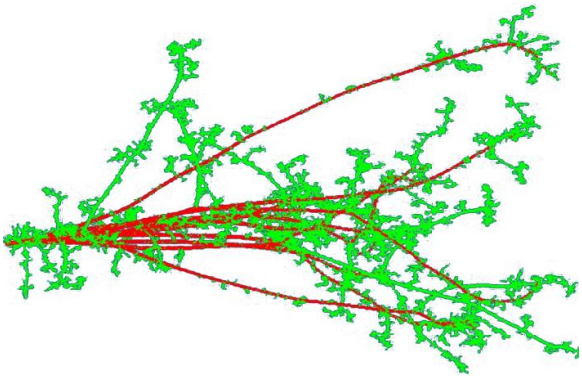

Fig.4 10 trajectories of 1***MeV*** Kr ions in pure iron obtained by the visualization tool of Deeper.

Using the OpenGL-based 3D visualization tool of Deeper code, the trajectories produced by 10 Krypton ions with energy of 1***MeV*** are presented in Fig.4. The red lines are the trajectories of Kr ions and the green lines are trajectories of secondary ions (recoil atoms), which can reflect the generation of damage cascade.

To test the reliability of the Deeper code used in ion simulation, statistic parameters are obtained and compared with the latest version of SRIM (SRIM-2013).The depth distribution of ions can reflect the accuracy of all models used in Deeper, we simulated the depth distribution of light ions (Hydrogen) and heavy ions (Krypton) with a same energy of 1***MeV*** in pure iron. Using SRIM-2013, the depth distribution of the same condition was also produced and comparison was made. The results are shown in Fig. 5.

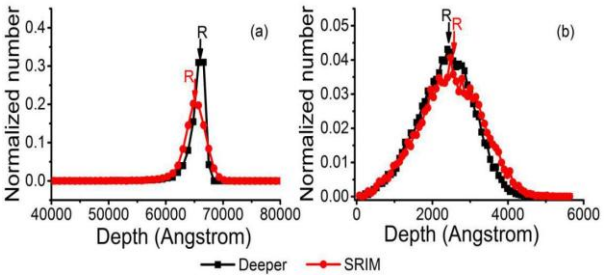

Fig.5 he depth distribution of ions in pure iron：(a)1***MeV*** Hydrogen ions; (b)1***MeV*** Krypton ions.

The depth profiles have a Gaussian-like distribution, which is caused by the random process of ion transportation. The parameter of range is defined as the depth where the ions stop with biggest probability, marked by an arrow(R) in Fig 4. We calculated the range of four kinds of ions in pure iron as a function of energy. The results from Deeper and comparison with SRIM are shown in Fig.6.

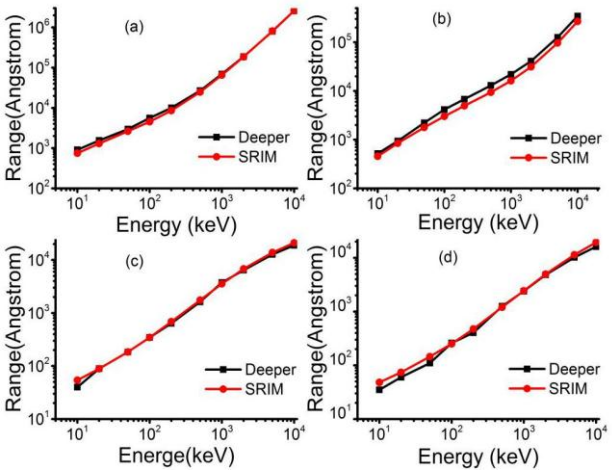

Fig.6 the range of ions in pure iron obtained by Deeper and SRIM as a function of energy of ions: (a) H, (b) He, (c) Fe and (d) Kr.

From the Fig.6 we can see good agreements of the range calculated by Deeper with the results from SRIM in a wide range of ion energy (from 10***keV*** to 10 ***MeV***). The results prove the good reliability of the

models used in Deeper, and confirm that the Deeper code has good performance in ion transporting simulation, which is essential for damage simulation. Using the function of simulating ion trajectories, Deeper can be used in the research based on ion interaction with solid materials, such as ion implanting, back scattering analyzing and ion sputtering.

3.3 Damage simulation using Deeper code

The primary damage generation induced by ions in materials is far beyond the limitation that any kinds of experimental approach can observe due to the very short time (a few tens of femto seconds) and small dimensions (size of mono atom). So using the simulation approach to investigate the primary generation plays a very important role in radiation damage research. Primary damage is often translated into DPA, which can reflect the damage level of materials, to calibrate the radiation dose in experiments. In multi-scale modeling, the information of primary damage is used as input data to other scale simulating tools. Deeper can produce both statistic results and detailed information of every defects.

The depth distributions of defects produced by 1***MeV*** Hydrogen ions and Krypton ions are presented in Fig.7.

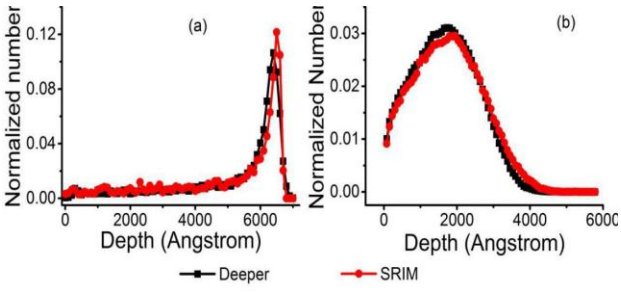

Fig. 7 vacancy profile of (a) 1***MeV*** Hydrogen ions and (b) 1***MeV*** Krypton ions in pure iron.

The comparison with SRIM-2013 is also presented in Fig.7 and quite good agreements can be found. Compared with the depth distribution of ion obtained in the same condition in Fig.5, a shallower peak region can be found in damage profile. This difference indicates that damage production has more close relationship with the energy deposited by nuclear collision than the position where ions stop. Figure 8 confirms this conclusion by plotting the profiles of damage production, ions, total energy deposit and energy deposited by nuclear collisions. The data of Fig. 8 come from the simulation of 1***MeV*** Hydrogen and Krypton ions in iron carried out by Deeper. To make data comparable, every kind of data is normalized to ensure that the highest peak equal to 1.0.

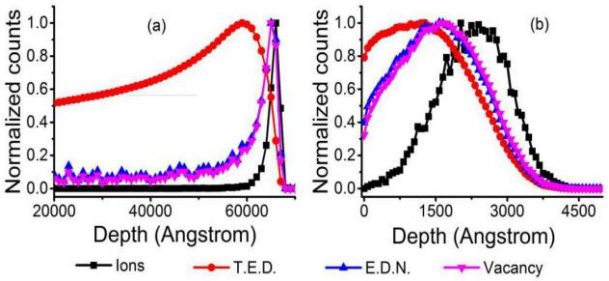

Fig. 8 the profiles of ions, total energy deposit(T.E.D.), energy deposited by nuclear collisions(E.D.N.) and vacancy simulated by Deeper. All data come from Deeper simulation of iron irradiated by (a) 1***MeV*** Hydrogen ions and (b) 1***MeV*** Krypton ions.

In Fig.8, the curve of ions stands for the ion profile, which is the same as the plot in Fig.5. Obvious Bragg peak can be found in the plot of total energy deposit. Total energy deposit can be divided into two parts: one is caused by collisions with electrons and the other is caused by nuclear collisions with nucleus. The energy loss by electronic collisions plays a dominating role with a total amount more than 100 times than the energy lost by nuclear collisions. The two kinds of energy loss have different profiles and the nuclear energy loss spread to a deeper depth. Although nuclear energy loss is only a small fraction of total energy loss, most of it can be transferred to crystal lattice atoms and cause damage. The distribution of vacancy (damage) nearly follows the results of nuclear energy loss and has less relationship with total energy deposit. Ions will travel deeper than the vacancy with energy lower than the displacement threshold when ions cannot produce damage but can keep transporting. The profile of damage in Fig.8 is a 1-D distribution which ignores the straggling of ions. 2-D distributions of damage are presented in Fig 9, which can give better understanding of primary damage induced by ion in materials.

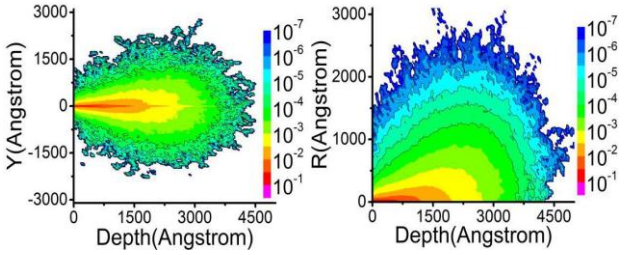

Fig. 9 (a) 2D primary damage distribution at *Z=0*;(b) primary damage distribution as a function of depth and distance to *X*-axis.

Figure 9 shows the 2-D distribution of primary damage produced by 1***MeV*** Krypton in iron. The ion bombard the specimen at the same position of (*0,0,0*) and with a direction along *X* axis. The primary damage with a unit of per ion per cubic nano meters was normalized by the total number of ions and the volume. In part (a), a slice of materials at *Z=0* was chosen to show the cross section of damage in specimen. In part (b), the distance of every defect to the bombarding direction was calculated and all defects were sorted by the depth and this kind of distance. By normalizing the defects number by the volume(can be translated into number of atoms per unit volume), the contours in Fig.9 can reflect the DPA distribution in a 2D manner. Although a peak damage region in 1D damage profile can be found, we must be careful to use the peak damage. It only valid under the condition that the area of radiated specimen is bigger the straggling of ions at the lateral direction.

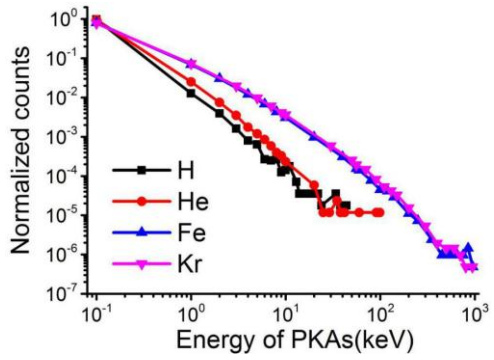

Fig. 10 the spectrum of PKA produced by 1***MeV*** ions in pure iron

To damage theory, the defects evolution differs greatly when the energy of PKAs varies[26]. For very low energy PKAs, only F-pairs exist while cluster will occur as the energy of PKAs increases. The energy spectrum of PKAs generated by different ions with same energy of 1***MeV*** are shown in Fig.10. To make the results comparable, all data are normalized by the number of PKAs. The PKAs produced by heavy ion have wider energy distribution. PKAs with energy lower than 100eV can only cause other atom displaced with very low efficiency. For the four kinds of ions, highly energized PKAs compose a very small fraction of total PKAs, but play much more important role in damage evolution because they will produce big cascades which cannot be recombined fully like F-pairs do. The debris of big cascade will form permanent damage structures during longtime evolution. The heaver the ions is, the more serious damage will be produced.

4 Conclusion

A code can be used to simulate ion trajectories and primary displacement damage in amorphous solid materials is presented in this paper. By using the geometrical relationship in CM system to process the nuclear elastic collisions and continuum inelastic energy loss based on experimental data to deal with electronic interaction, this code can simulate the interaction between ions and materials with good accuracy and efficiency. To test the reliability of this code, we compared the ion depth distribution, the range and damage profile of light ions and heavy ions in iron with the results from SRIM-2013. We also utilized it to simulate the displacement damage induced by Krypton ion in iron to get the 2-D damage distribution. The spectrum of PKA indicates that very different cascades can be produced by light ions and heavy ions with various energy. At present time, this code ignores the generation of all secondary particles excluding the recoil atoms, such as secondary electrons, Auger electrons and X-rays, so it is invalid for many specific applications which use secondary effect, like surface analyzing and PIXE (particle induced X-ray emission). The function of simulating generation of secondary particles can be added to this code if needed in future. Due to its good performance in simulating the transporting and damage generation of ions in materials, the code was integrated into a comprehensive damage modeling tool, the Deeper code, which will be released for free in very near future.

Acknowledgement

The authors would like to thank Dr. L. Shao, professor of Texas A&M university, for his very valuable discussion and suggestion on models selection and programming. This work is supported by the Fundamental Research Funds for the Central Universities of China (HEUCF151503).

References

[1] MICHAEL, Nastasi, MAYER, J. W., and WANG, Yongqiang: Ion Beam Analysis, Fundamentals and Applications, New York: CRC Press of the Taylor & Francis Group, 2015: 3-9

[2] HELLBORG, Ragnar, WHITLOW, H. J., and ZHANG, Yanwen: Ion Beams in Nanoscience and Technology, New York: Springer, 2009: xix-xxiii

[3] DEMIDCHIK, Vadim, and MAATHUIS, Frans: Ion Channels and Plant Stress Responses, New York: Springer, 2009, 2-14

[4] WAS, G. S.: Fundamentals of Radiation Materials Science, Berlin-Heidelberg, Springer, 2007, 133-136

[5] ALLEN, T. R., STOLLER, R. E., and YAMANAKA, S.: Comprehensive Nuclear Materials, Volume 1: Basic Aspects Of Radiation Effects In Solids/Basic Aspects Of Multi-Scale Modeling, Netherland, Elsevier, 2012, 393-411

[6] http://www.fluka.org/fluka.php

[7] http://geant4.web.cern.ch/geant4/

[8] ROBINSON, M. T.: Nucl. Instrum. Methods. 1990, B48, 408-413.

[9] ZIEGLER, J. F., BIERSACK, J. P., and ZIEGLER, M. D.: Nucl. Instrum. Methods, 2010, B268, 1818-1823

[10] http://www.srim.org/

[11] MAYER, M.: SIMNRA, a Simulation Program for the Analysis of NRA, RBS and ERDA, Proceedings of the 15th International Conference on the Application of Accelerators in Research and Industry, J. L. Duggan and I.L. Morgan (eds.), American Institute of Physics Conference Proceedings, 1999, 475-541

[12] http://www.hzdr.de/db/Cms?pOid=21578&pNid=0

[13] ROBINSON, M. T., and TORRENS, L. M.: Phys. Rev. ,1974, B9, 5008-5024

[14] IGNACIO, M. *et al.*, Comp. Phys. Comm., 2013,184 2703–2710

[15] BIERSACK, J. P., and HAGGMARK, L.G.: Nucl. Instrum. Methods, 1980,174, 257-269

[16] LINDHARD, J.and SCHARFF, M.: Phys. Rev., 1961, 124 ~ 128.

[17] GOLOVCHENKO, J. A., COX, D. E. and GOLAND, A. N.: Phys. Rev., 1982, B 26, 2335

[18] TAI, H., BICHSEL, H., WILSON, J. W., SHINN, J. L., CUCINOTTA, F. A., and BADAVI, F. F.: Comparison of Stopping Power and Range Databases for Radiation Transport Study, NASA Technical Paper 1997, 3644

[19] ANDERSEN, H. H. and ZIEGLER, J.F.: Hydrogen - Stopping Powers and Ranges in All Elements,vol. 3 of The Stopping and Ranges of Ions in Matter.New York, Pergamon Press, 1977, 16

[20] ZIEGLER, J.F.: Helium - Stopping Powers and Ranges in All Elements, vol. 4 of the Stopping and Ranges of Ions in Matter. New York:Pergamon Press, 1977, 66

[21] ZIEGLER, J. F., BIERSACK, J.P., and ZIEGLER, M. D.: The Stopping and Range of Ions in Matter, Morrisville, Lulu Press,2010, chp.3

[22] ZIEGLER, J.F., BIERSACK, J.P., and LITTMARK, U.: Stopping and Range of Ions in Solids, Vol. 1 of "The Stopping and Ranges of Ions in Matter", New York, Pergamon Press, 1985, 60.

[23] MATSUMOTO, M. and NISHIMURA, T.: Mersenne Twister, A 623-Dimensionally Equi-distributed Uniform Pseudo- Random Number Generator, ACM Transactions on Modeling and Computer Simulation, 1998, Vol. 8, No. 1, 3-30

[24] http://opengl.en.softonic.com/

[25] LINDHARD, J., SCHARFF, M., SCHIOTT, H. E., and DAN, K.: Vidensk. Selsk. Mat. Fys. Medd. 1963, 33, 14.

[26] WAS, G.S. and ALLEN, T.: Mater. Char., 1994, 32, 239-255